SUPPLEMENTARY FIGURES AND LEGENDS

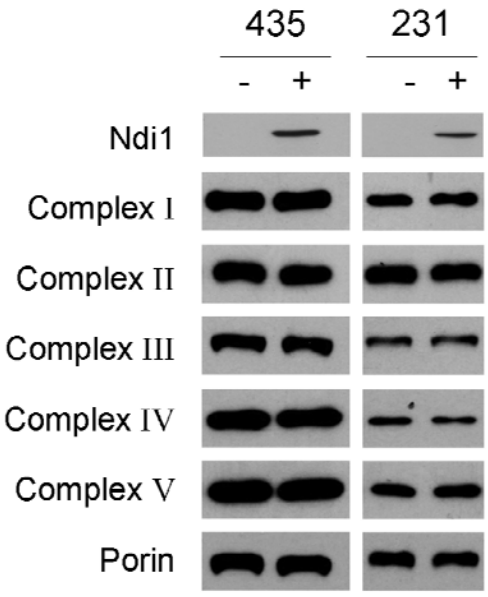

Figure S1. Ndi1 expression does not alter mitochondrial complex stoichiometry in human breast cancer cells

Western blot analysis of Ndi1 protein and mitochondrial complexes to assess the stoichiometry of complexes I-V in MDA-MB-435 (435) and MDA-MB-231 (231) cells +/- transduction with Ndi1. Detected subunits: NDUFA9 (complex I), SDHA (complex II), UQCR2 (complex III), COXI (complex IV), ATP5A1 (complex V), Mitochondrial porin (VDAC1) shown as loading control. For all representative immunoblots, lanes separated by white lines were run on the same gel but were noncontiguous.

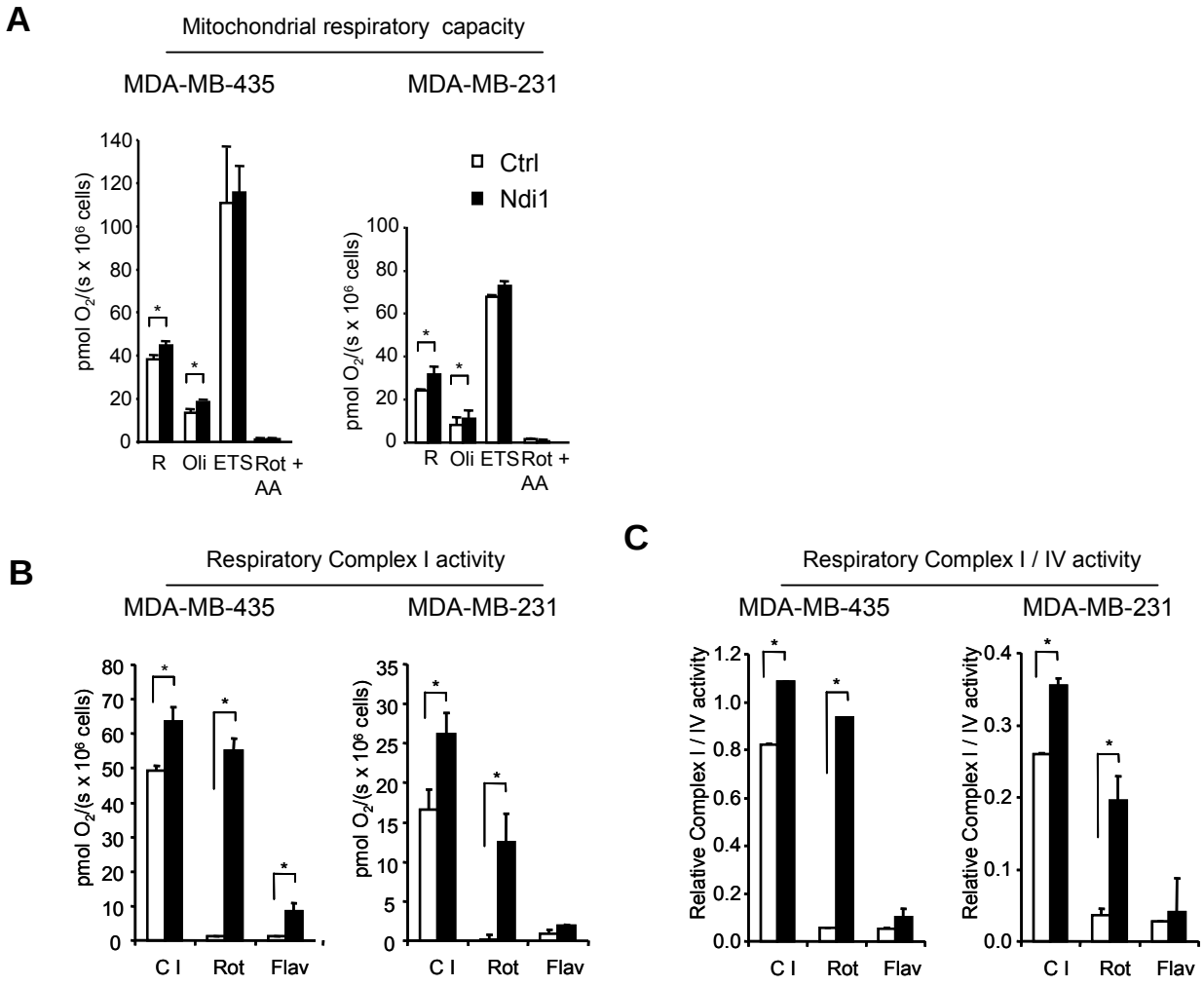

Figure S2. Ndi1 expression specifically enhances complex I activity without altering the maximum capacity of the electron transfer system (ETS)

(A) Mitochondrial respiratory capacity. Control (white) vs Ndi1 expressing (black) MDA-MB-435 or MDA-MB-231 cells ($2x10^6$) were collected in complete media and respiration measured by high-resolution respirometry at 37 °C in a 2 ml chamber using an Oroboros Oxygraph series D and DatLab software (Oroboros Instruments, Innsbruck, Austria). First, routine respiration (R) was measured in intact cells in complete medium. After reaching stead-state respiratory flux, ATP synthase was inhibited with oligomycin (Oli) (2 µg/ml). This leads to an increase in mitochondrial membrane potential due to continued proton pumping by complexes I, III, and IV into the mitochondrial intermembrane space, after proton flow through ATP synthase is inhibited. Respiration in this state is due to proton leakage (Leak state). In this Leak state, respiration was uncoupled from oxidative phosphorylation by stepwise addition of carbonylcyanide p-trifluoromethoxyphenylhydrazone (FCCP) (1µM increments, range 4-6 µM) until maximal respiratory capacity of the electron transfer system (ETS) was reached. Finally, respiration was inhibited by sequential addition of rotenone (Rot) and 2.5 µM antimycin A (AA). The results reflect maximal mitochondrial capacity of the ETS, quantified as oxygen consumption in uncoupled mitochondria (*

P<0.05). **(B,C)** Respiratory mitochondrial complex I activity. Oxygen consumption of digitonin-permeabilized control (white) vs Ndi1 (black) expressing MDA-MB-435 or MDA-MB-231 cells ($4x10^6$) was measured by high-resolution respirometry at 37 °C in a 2 ml chamber as described [1, 2]. Briefly, cells were collected into respiration medium (20 mM HEPES, 2 mM potassium phosphate, both adjusted to pH 7.1, 250 mM sucrose, 10 mM $MgCl_2$ and 1 mM ADP), permeabilized with digitonin for 1 min, washed with respiration medium, and then added to the chamber prefilled with respiration medium. Respiration was analyzed after adding complex I specific substrates malate and glutamate (5mM each) (C I). Mammalian complex I dependent respiration was measured after inhibition with rotenone (Rot) (5 μM). Ndi1 mediated respiration was measured after incubation with flavone (0.3 mM) (Flav), a partial Ndi1 inhibitor [2]. Complex III was then inhibited with 2.5 μM antimycin A. **(B)** Respiratory complex I activity is expressed as pmol of oxygen consumed/second/10^6 cells. **(C)** Respiratory complex I activity expressed relative to complex IV activity. Complex IV activity was measured after adding 2 mM ascorbate and 0.5 mM TMPD (tetramethyl-p-phenylenediamine).

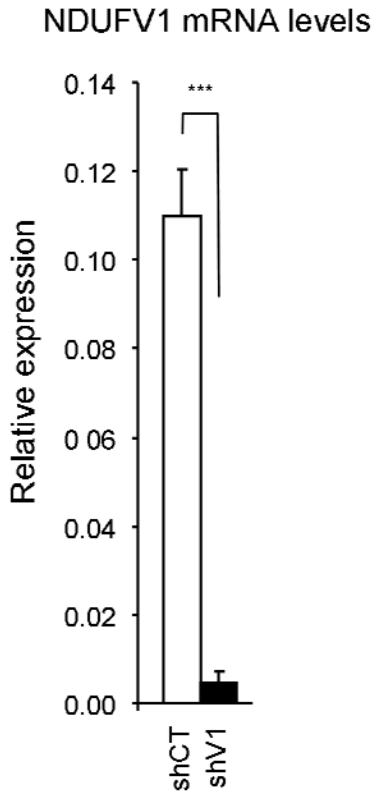

Figure S3. Reduction of NDUFV1 expression by shNDUFV1 knockdown

Stable NDUFV1 knockdown (shV1) in MDA-MB-435 parental cells decreased NDUFV1 mRNA levels by 96 % compared to controls transduced with scrambled shRNA (shCT). NDUFV1 mRNA expression levels were analyzed by quantitative real time PCR relative to GAPDH (***P<0.001) (n = 3).

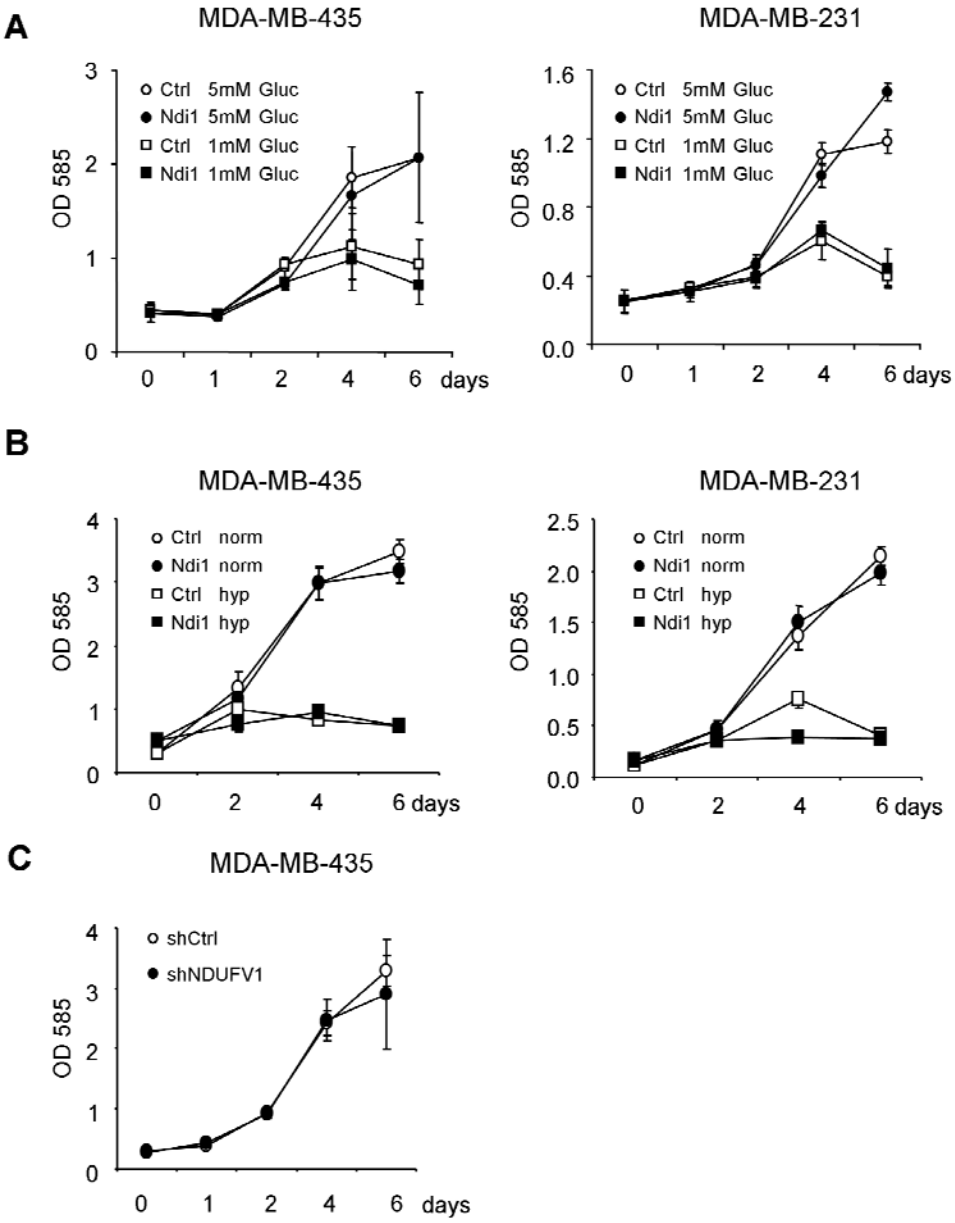

Figure S4. Modulation of complex I activity does not affect tumor cell proliferation *in vitro*

(A) Proliferation of control (Ctrl) vs Ndi1 expressing MDA-MB-435 or MDA-MB-231 cells cultured in 5 mM or 1 mM glucose under normoxic conditions (21% oxygen). **(B)** Proliferation of control (Ctrl) vs Ndi1 expressing MDA-MB-435 or MDA-MB-231 cells cultured in 5 mM Glucose under normoxia (21% Oxygen) vs hypoxia (<1% Oxygen). **(C)** Proliferation of control (shCtrl) vs NDUFV1 knockdown MDA-MB-435 (shNDUFV1) cells cultured in 5 mM Glucose under atmospheric oxygen conditions (21% oxygen). Proliferation was measured on day 1, 2, 4 and 6 based on crystal violet staining and is expressed as optical density (OD) at 585 nm (n = 3).

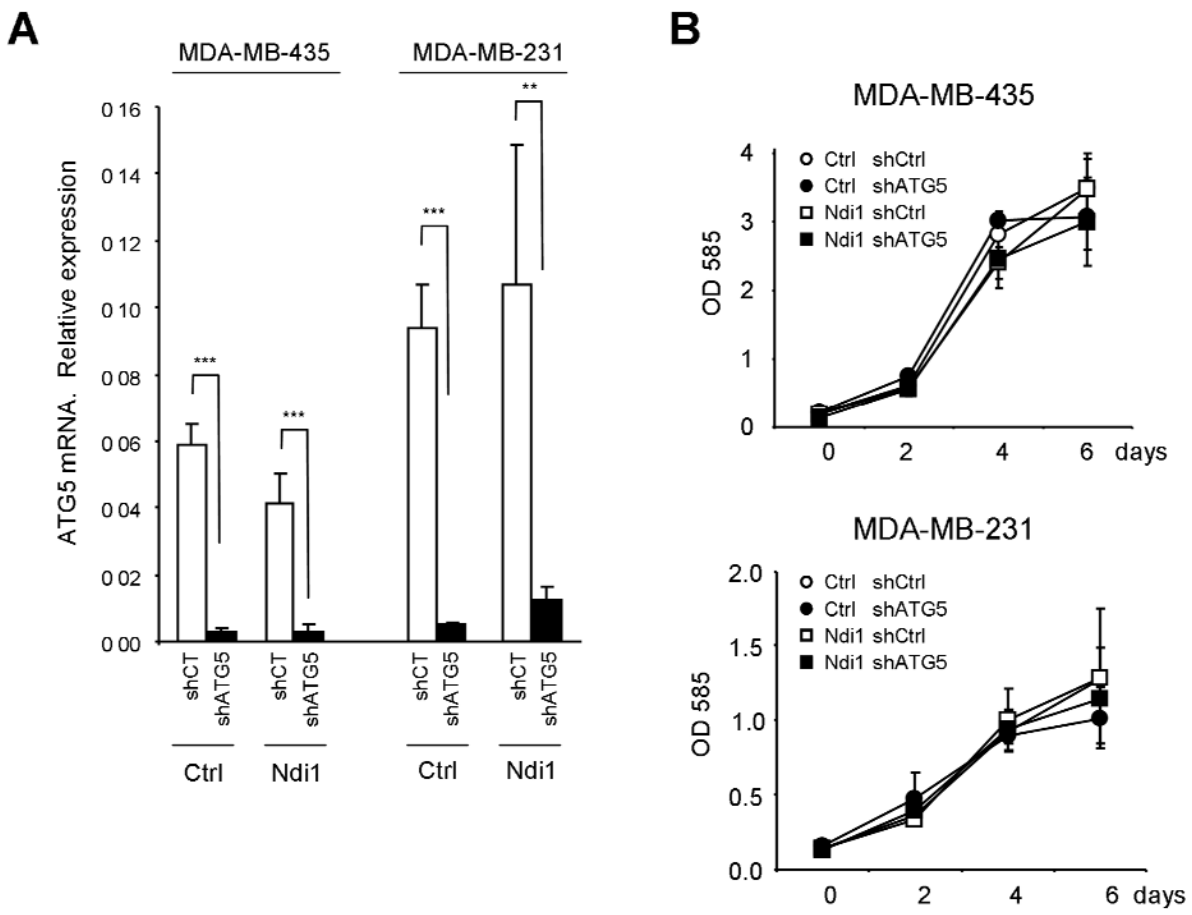

Figure S5. ATG5 knocked down does not affect tumor cell proliferation *in vitro*

(A) Stable ATG5 knockdown (shATG5) significantly reduced ATG5 mRNA levels in control (Ctrl) and Ndi1 expressing MDA-MB-435 and MDA-MB-231 cells. Knockdown efficiency for MDA-MB-435 was 95 % in control and 93 % in Ndi1 expressing cells; knockdown efficiency for MDA-MB-231 was 95 % in control and 88 % in Ndi1 expressing cell based on comparison of knockdown vs scrambled shRNA transduced controls (shCT). ATG5 mRNA levels were analyzed by real time PCR and expressed relative to GAPDH (***P<0.001) (n = 3). **(B)** Proliferation of control (shCtrl) or ATG5 knockdown (shATG5) MDA-MB-435 or MDA-MB-231 cells cultured with 5 mM glucose under normoxia (21% Oxygen). Proliferation was measured on day 2, 4 and 6 based on crystal violet staining and is expressed as optical density (OD) at 585 nm (n = 3).

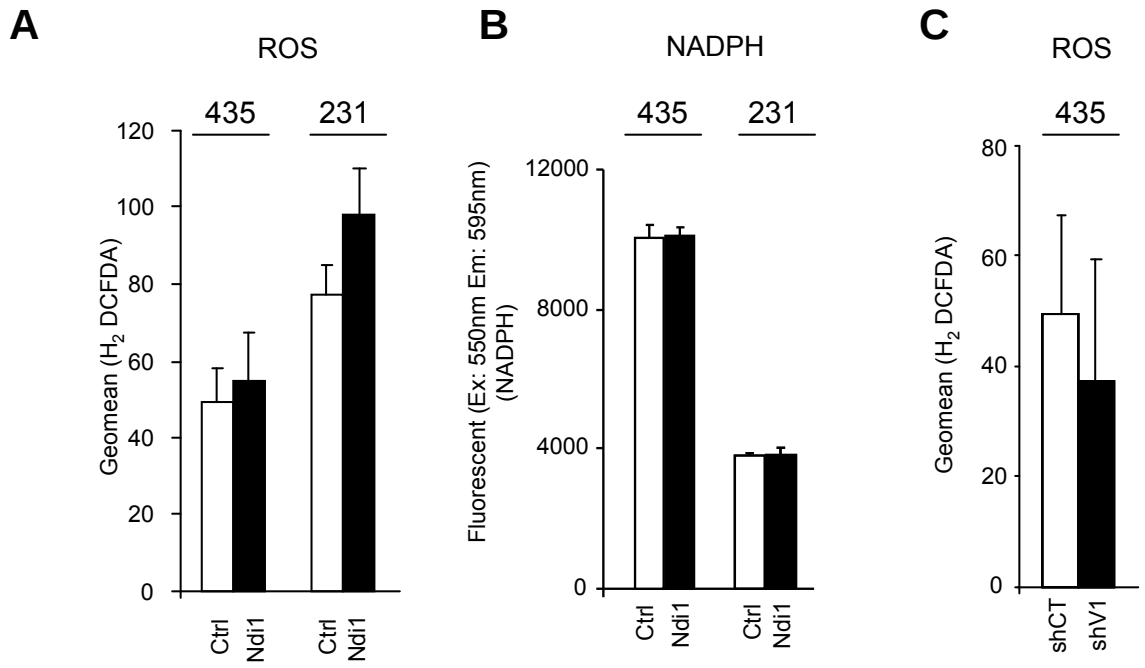

Figure S6. Modulation of complex I by Ndi1 does not change ROS levels and the NADPH REDOX state

(A) Ndi1 expression did not significantly change ROS levels in MDA-MB-435 or MDA-MB-231 cells. ROS levels (hydrogen peroxide) were detected with 2′-,7′-dichlorodihydrofluorescein diacetate (H2DCFDA) and measured by flow cytometry. Cells were incubated with 0.5 μM H2DCFDA for 30 min at 37 ºC in serum-free EMEM and washed twice with PBS. Data from 10,000 events per sample were collected and analyzed by measuring FL-1 fluorescence. **(B)** Ndi1 expression did not change NADPH levels. NADPH was extracted from $1x10^6$ cell and NADPH levels determined using a fluorescent $NADP^+$/NADPH detection kit (Cell technology, Inc). **(C)** NDUFV1 knockdown (shV1) in MDA-MD-435 cells did not significantly change ROS levels.

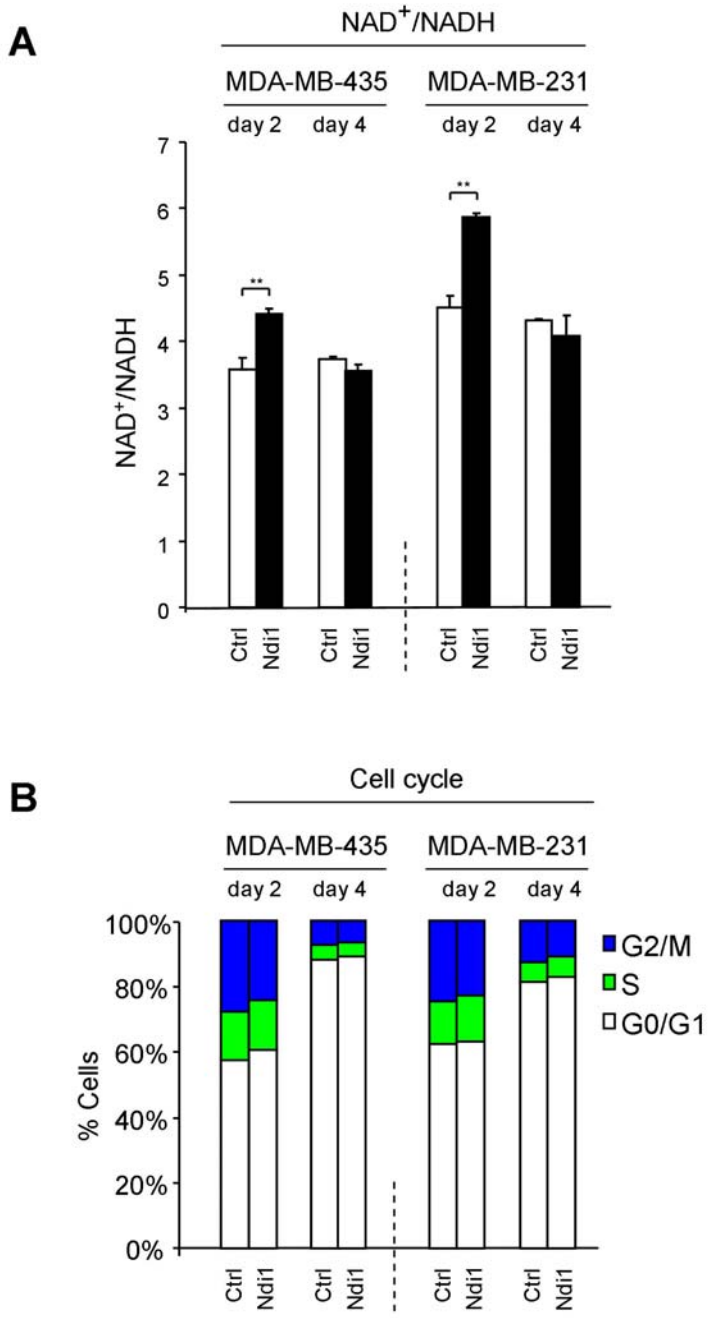

Figure S7. Effect of Ndi1 expression on NAD$^+$/NADH levels during cell growth

(A) Increased NAD$^+$/NADH ratios in Ndi1 expressing MDA-MB-435 and MDA-MB-231 cells (Ndi1) were measurable *in vitro* during logarithmic cell growth. Whole cell extracts were analyzed after 2 or 4 days of culture in complete medium. Cells were subconfluent on day 2 and confluent on day 4. Control cells were transduced with empty vector (Ctrl). Groups were compared by unpaired two-tailed Student's *t*-test in n=2 independent experiments (*P<0.05, **P<0.01). **(B)** Cell cycle analysis of control or Ndi1 expressing MDA-MB-435 and MDA-MB-231 cells after 2 or 4 days of culture in complete medium. Cell cycle was measured by flow cytometry (n=2 independent analyses). Cells were fixed in ice cold 70% ethanol, washed with PBS and incubated with 50 µg/ml propidium iodide and 100 µg/ml RNAse A for 30 minutes at 37°C. Data from 20,000 events per sample were collected by measuring FL-2 fluorescence.

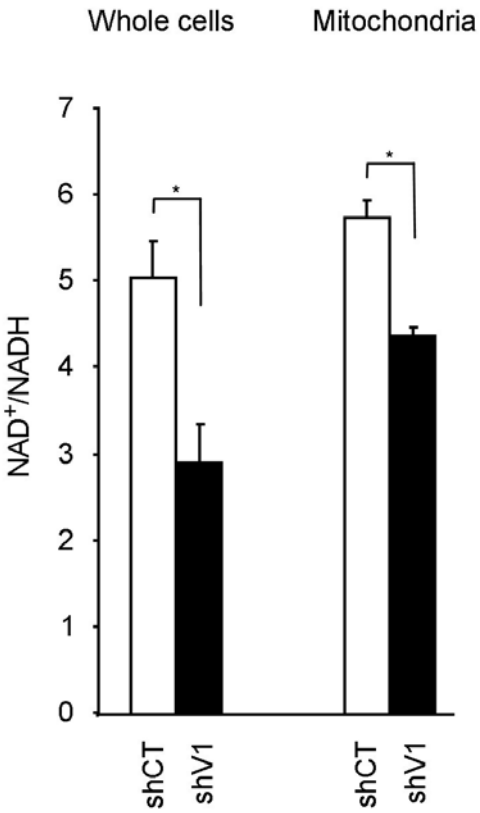

Figure S8. NDUFV1 knockdown reduces NAD^+/NADH ratios in MDA-MB-435 tumor cells

NAD^+/NADH ratios in whole cell or mitochondrial extracts of MDA-MB-435 control (Ctrl) vs NDUFV1 knockdown (shV1) cells, cultured under standard conditions.

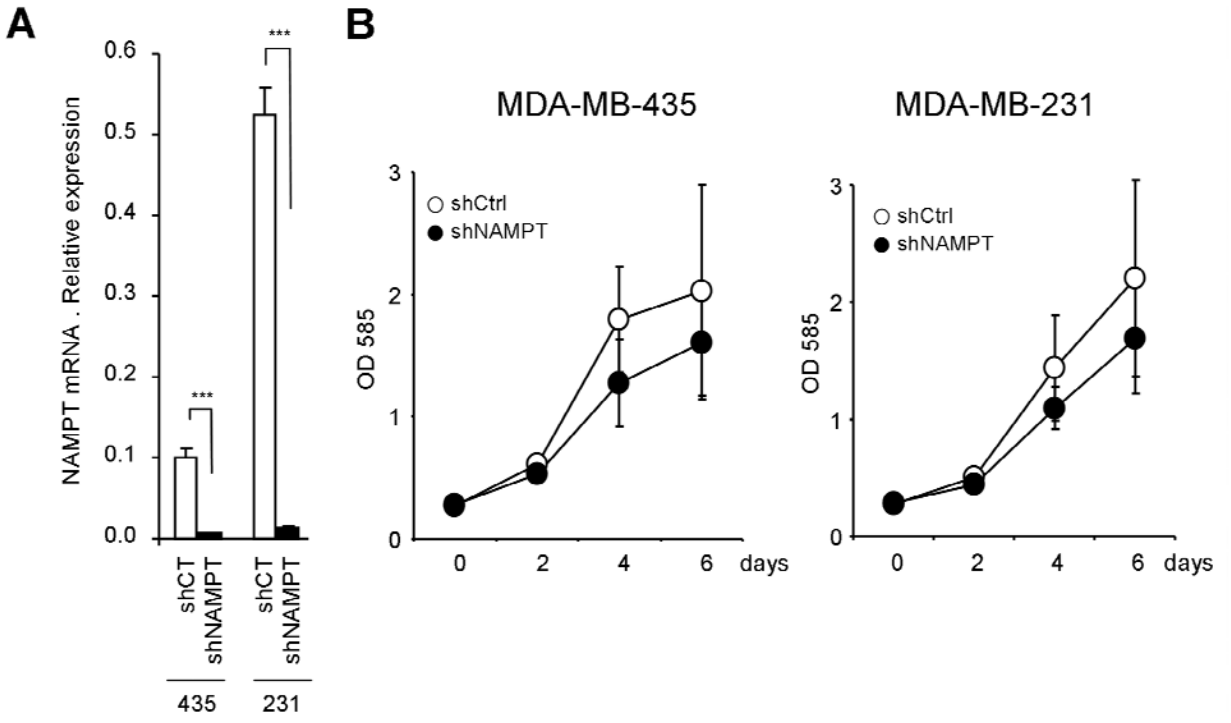

Figure S9. NAMPT knock down does not affect tumor cell proliferation *in vitro*

(A) NAMPT knockdown (shNAMPT) reduced NAMPT expression by 92 % in MDA-MB-435 cells, and by 97 % in MDA-MB-231 cells, compared to controls transduced with scrambled shRNA (shCT). NAMPT mRNA levels were analyzed by real time PCR and are expressed relative to GAPDH (***P<0.001) (n = 3). **(B)** Proliferation of control (shCtrl) vs NAMPT knockdown (shNAMPT) MDA-MB-435 or MDA-MB-231 cells cultured with 5 mM glucose under normoxic conditions (21% oxygen). Proliferation was measured on day 2, 4 and 6 based on crystal violet staining and is expressed as optical density (OD) at 585 nm (n = 3).

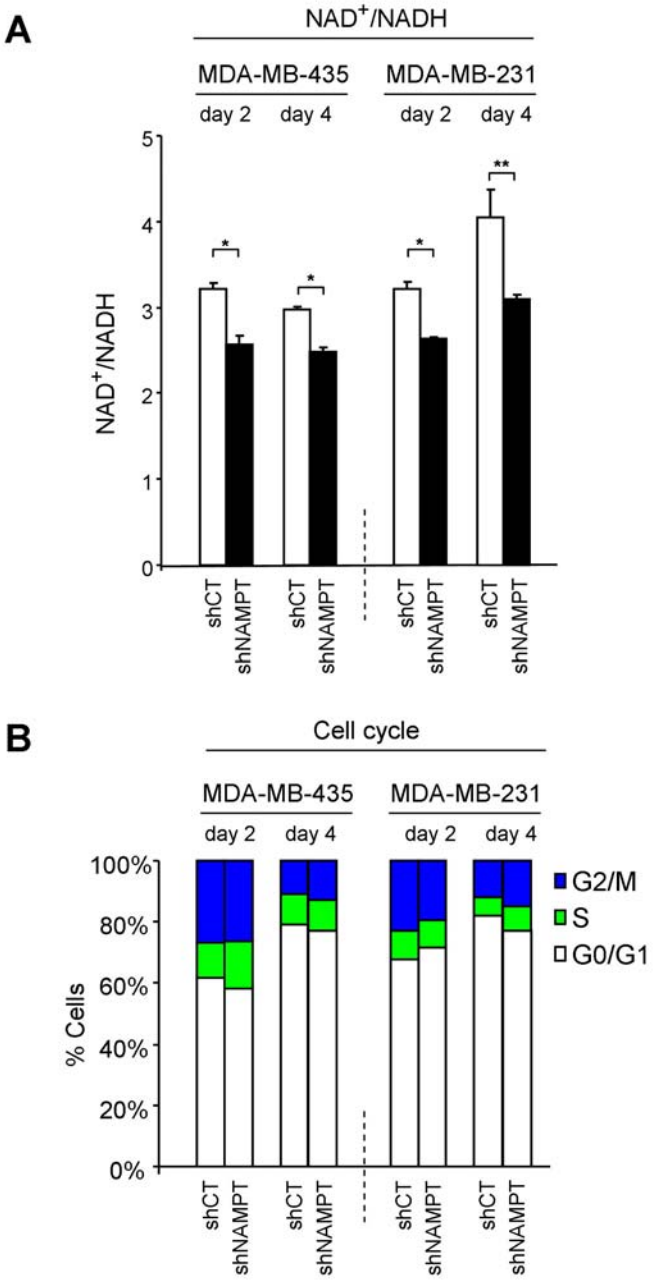

Figure S10. Effect of NAMPT knockdown on NAD$^+$/NADH levels during cell growth

(A) Interference with NAD$^+$ synthesis and recycling pathways reduces NAD$^+$/NADH ratios. Knockdown of NAMPT in MDA-MB-435 and MDA-MB-231 cells (shNAMPT) decreased NAD$^+$/NADH ratios (whole cell extracts after 2 or 4 days of culture in complete medium. Cells were subconfluent on day 2 and confluent on day 4. Control cells were transduced with non-targeting control shRNA (shCT). Groups were compared by unpaired two-tailed Student's *t*-test in n=2 independent experiments (*P<0.05, **P<0.01). **(B)** Cell cycle analysis of MDA-MB-435 and MDA-MB-231 control (shCT) or NAMPT KD cells (shNAMPT) after 2 or 4 days of culture in complete medium. Cell cycle was measured by flow cytometry (n=2 independent analyses). Cells were fixed in ice cold 70% ethanol, washed with PBS and incubated with 50 µg/ml propidium iodide and 100 µg/ml RNAse A for 30 minutes at 37°C. Data from 20,000 events per sample were collected by measuring FL-2 fluorescence.

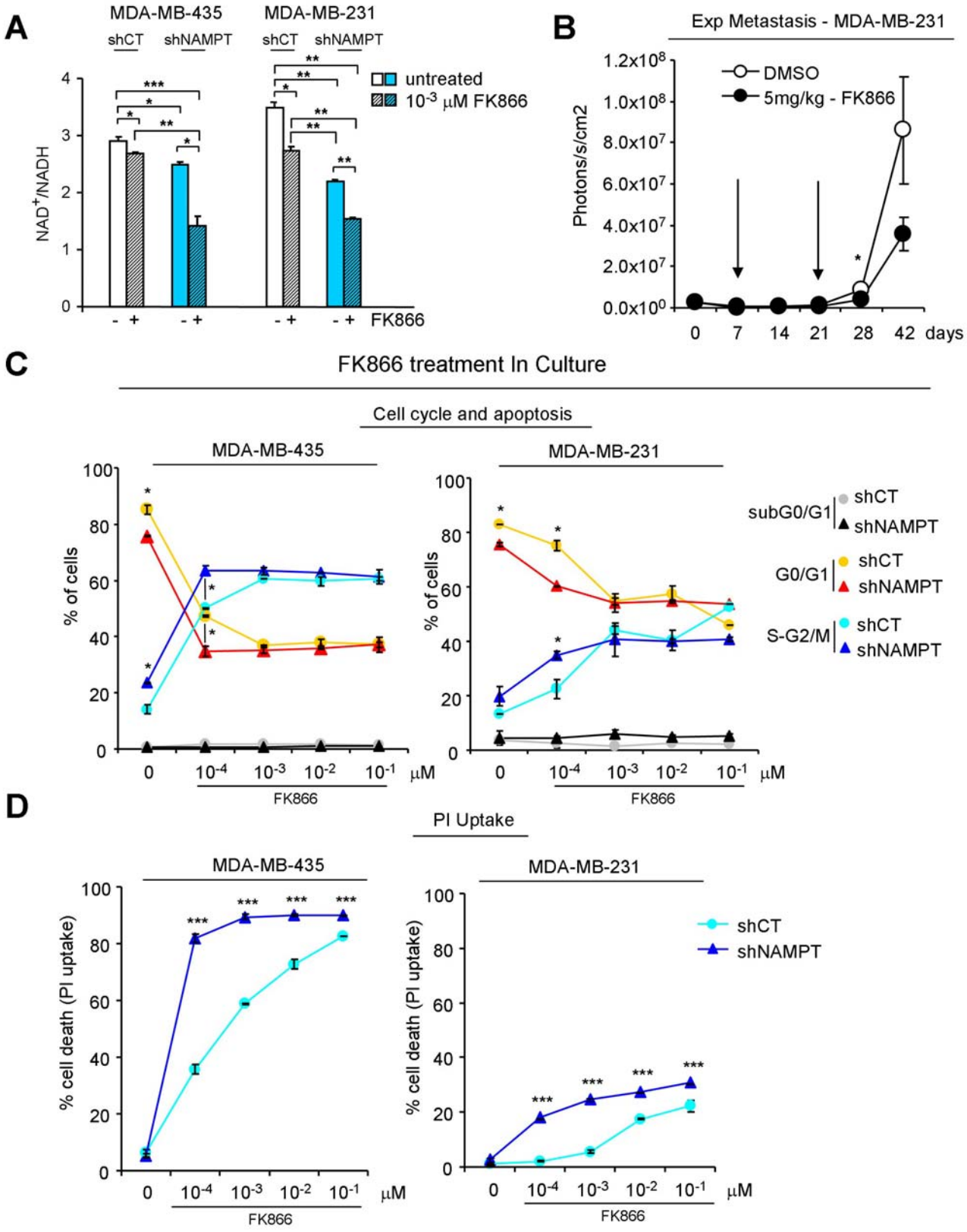

Figure S11. Pharmacologic inhibition of NAMPT interferes with experimental metastasis and induces S/G2 cell cycle arrest and necrosis *in vitro*

(A) Treatment with NAMPT inhibitor FK866 (FK) decreased the NAD^+/NADH ratio in cultured MDA-MB-435 and MDA-MB-231 control (shCT) or NAMPT knockdown cells (shNAMPT). NAD^+/NADH levels were

measured after 2 days of cell treatment with 10^{-3} μM FK866 (FK) in complete medium. Groups were compared by unpaired two-tailed Student's *t*-test in n=2 independent experiments (*P<0.05, **P<0.01, ***P<0.001).

(B) Animal treatment with NAMPT inhibitor FK866 (Sigma-Aldrich, MO) inhibits lung metastasis in experimental mice**.** SCID mice were i.v. injected with MDA-MB-231 parental cells ($2.5x10^5$) and treated with 5mg/kg FK866 i.p. every 12 hours during two 4-day cycles, starting the first cycle on day 7 and the second on day 21 post tumor cell injection. Controls received vehicle only (15% DMSO in PBS). Metastatic growth was measured by repeated non-invasive bioluminescence imaging (x-axes: time in weeks). Groups were compared by nonparametric Mann-Whitney test (* P<0.05, n = 6 /group).

(C) FK866 treatment induces S/G2 cell cycle arrest in MDA-MB-435 (left panel) and MDA-MB-231 (right panel) cells, particularly after NAMPT knockdown, but does not induce apoptosis. Cell cycle was measured by flow cytometry (n=2 independent analyses). Cells were fixed in ice cold 70% ethanol, washed with PBS and incubated with 50 μg/ml propidium iodide (PI) and 100 μg/ml RNAse A for 30 minutes at 37°C. Data from 20,000 events per sample were collected by measuring FL-2 fluorescence. (*P<0.05 by unpaired two-tailed Student's *t*-test). **(D)** FK866 treatment induces cell death in MDA-MB-435 (left panel) and MDA-MB-231 cells (right panel), particularly after NAMPT knockdown. Cell death was measured by flow cytometry based on loss of plasma membrane integrity indicated by PI uptake (n=2 independent analyses). Cells were washed with PBS and incubated with 5 μg/ml PI for 15 minutes at room temperature. Data from 10,000 events per sample were collected and by measuring FL-3 fluorescence.(***P<0.001 by unpaired two-tailed Student's *t*-test).

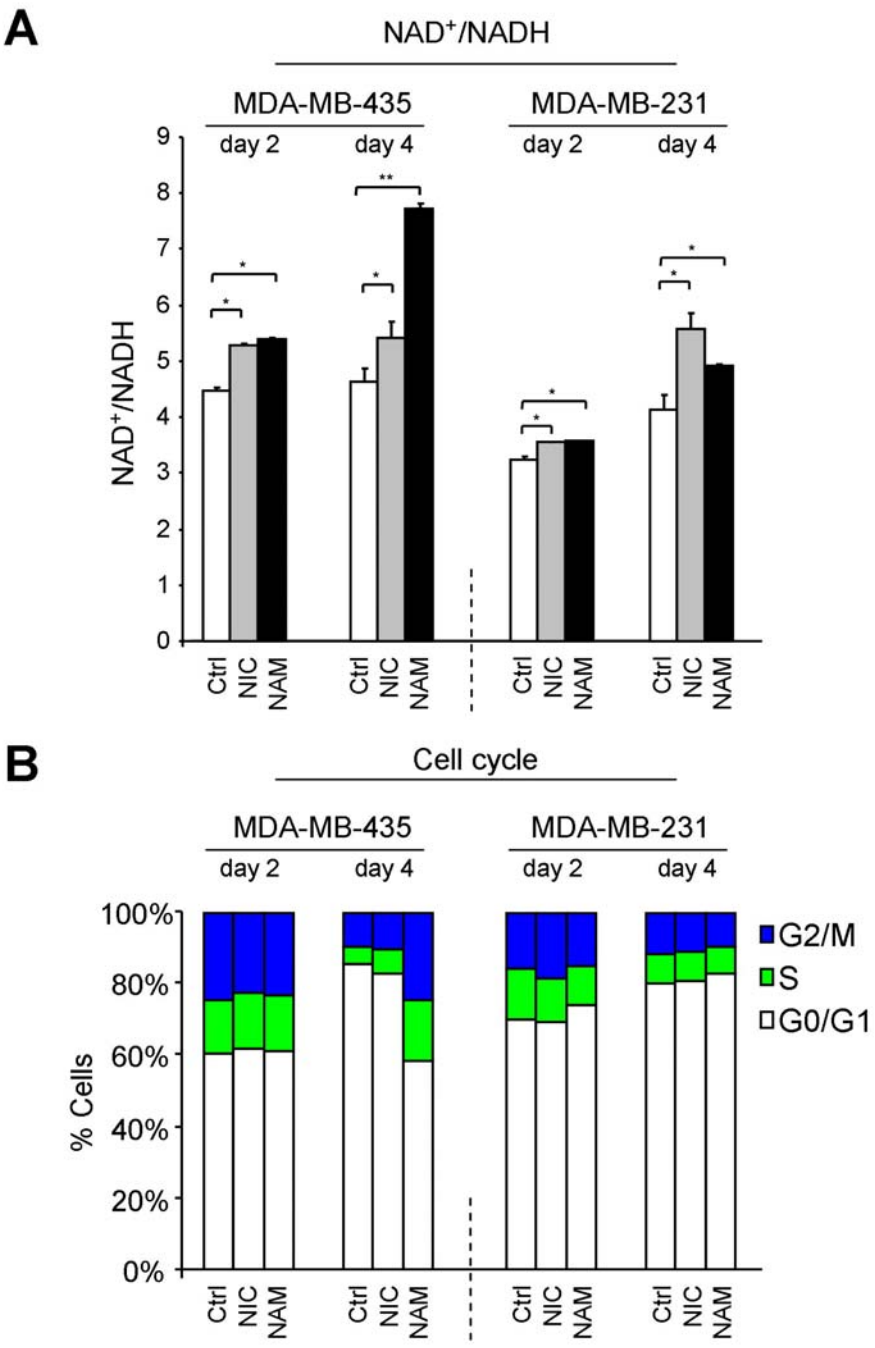

Figure S12. Effect of NAD$^+$ precursor treatment on NAD$^+$/NADH levels during cell growth

(A) NAD$^+$ precursor treatment enhances the NAD$^+$/NADH ratio in cultured MDA-MB-435 and MDA-MB-231 parental cells. NAD$^+$/NADH levels were measured after 2 and 4 days of cell treatment with 10 mM nicotinic acid (NIC) or nicotinamide (NAM) in complete medium. Groups were compared by unpaired two-tailed Student's *t*-test in n=2 independent experiments (*P<0.05, **P<0.01). **(B)** Cell cycle analysis of MDA-MB-435 and MDA-MB-231 parental cells treated with 10 mM NIC or 10 mM NAM during 2 or 4 days in culture in complete medium. Cell cycle was measured by flow cytometry (n=2 independent analyses). Cells were fixed in ice cold 70% ethanol, washed with PBS and incubated with 50 µg/ml propidium iodide and 100 µg/ml RNAse A for 30 minutes at 37°C. Data from 20,000 events per sample were collected by measuring FL-2 fluorescence.

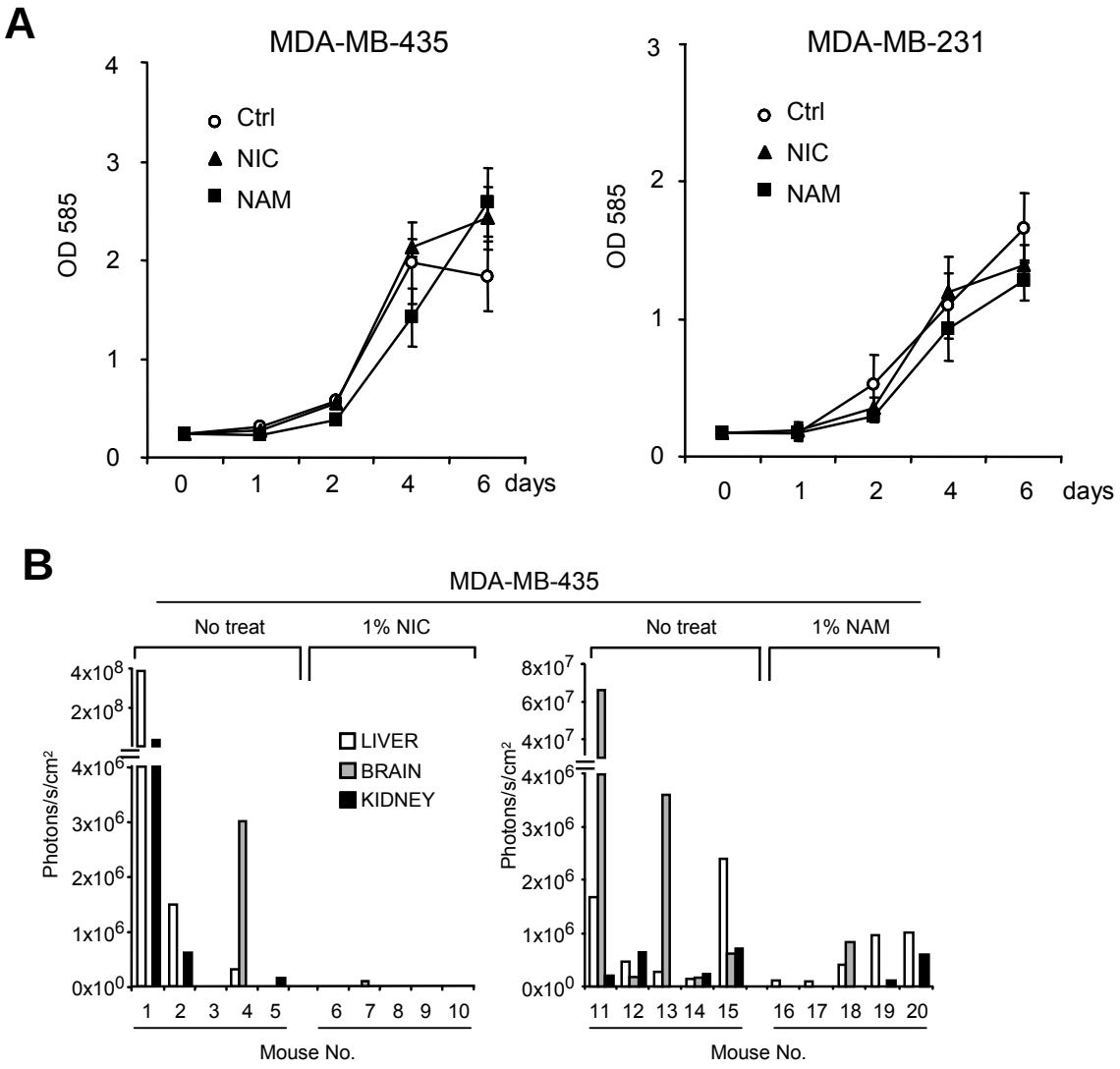

Figure S13. NAD$^+$ precursor treatment effects on proliferation and metastasis

(A) MDA-MB-435 or MDA-MB-231 parental cells were treated with nicotinic acid (NIC) or nicotinamide (NAM) (10 mM in each case) in complete growth medium, compared to controls grown without NAD$^+$ precursors. Proliferation was measured on day 1, 2, 4, and 6 by crystal violet staining (OD 585 nm) (n=3). **(B)** NAD$^+$ precursor treatment of experimental mice inhibits multiorgan metastasis. Metastatic burden was quantified in excised livers, brains and kidneys of individual mice by *ex vivo* organ imaging 5 weeks after i.v. injection of 2.5x10^5 MDA-MB-435 cells. Treated mice received NIC or NAM (1% in the drinking water throughout the experiment). Controls received no treatment (n=5/group).

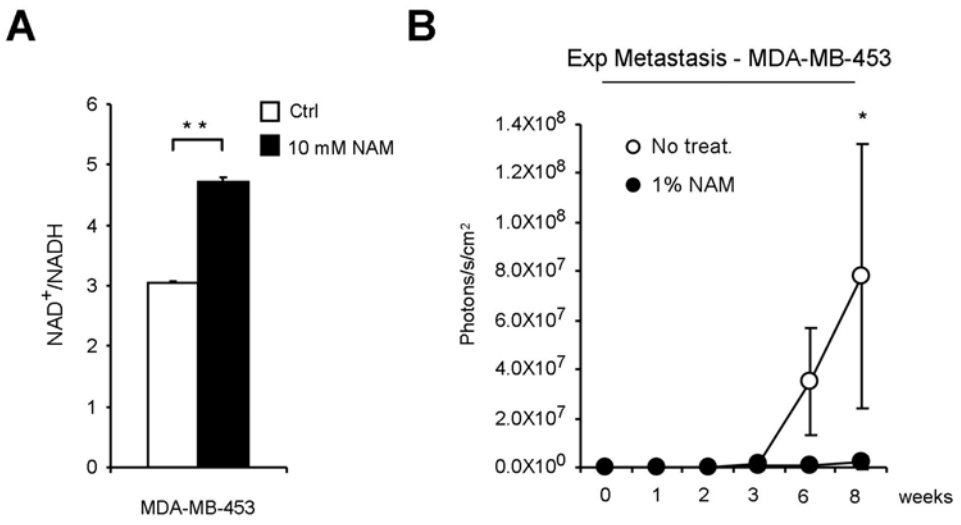

Figure S14. NAD^+ precursor treatment inhibits brain metastasis of MDA-MB-453 cells

(A) NAD^+ precursor treatment enhances the NAD^+/NADH ratio in cultured MDA-MB-453 parental cells. NAD^+/NADH levels were measured after 2 days of cell treatment with 10 mM nicotinamide (NAM) in complete medium. Groups were compared by unpaired two-tailed Student's *t*-test in n=2 independent experiments (**P<0.01). **(B)** NAD^+ precursor treatment of experimental mice inhibits brain metastasis**.** Mice injected with $2.5x10^5$ MDA-MB-453 parental cells into the left cardiac ventricle were treated with NAM (1% in the drinking water ad libitum throughout the experiment). Controls received no treatment (plain drinking water at same pH). MDA-MB-453 cells have a propensity to colonize the brain. To assess brain metastasis from MDA-MB-453 cells, mice were imaged directly after cardiac injection to validate routing to the brain by verifying tumor cell signal in the brain region and lack of signal in the lungs. This was achieved in 3/10 injected mice. Brain metastatic growth was measured by repeated non-invasive bioluminescence imaging (x-axes: time in weeks). Groups were compared by nonparametric Mann-Whitney test (n=3) (* P<0.05).

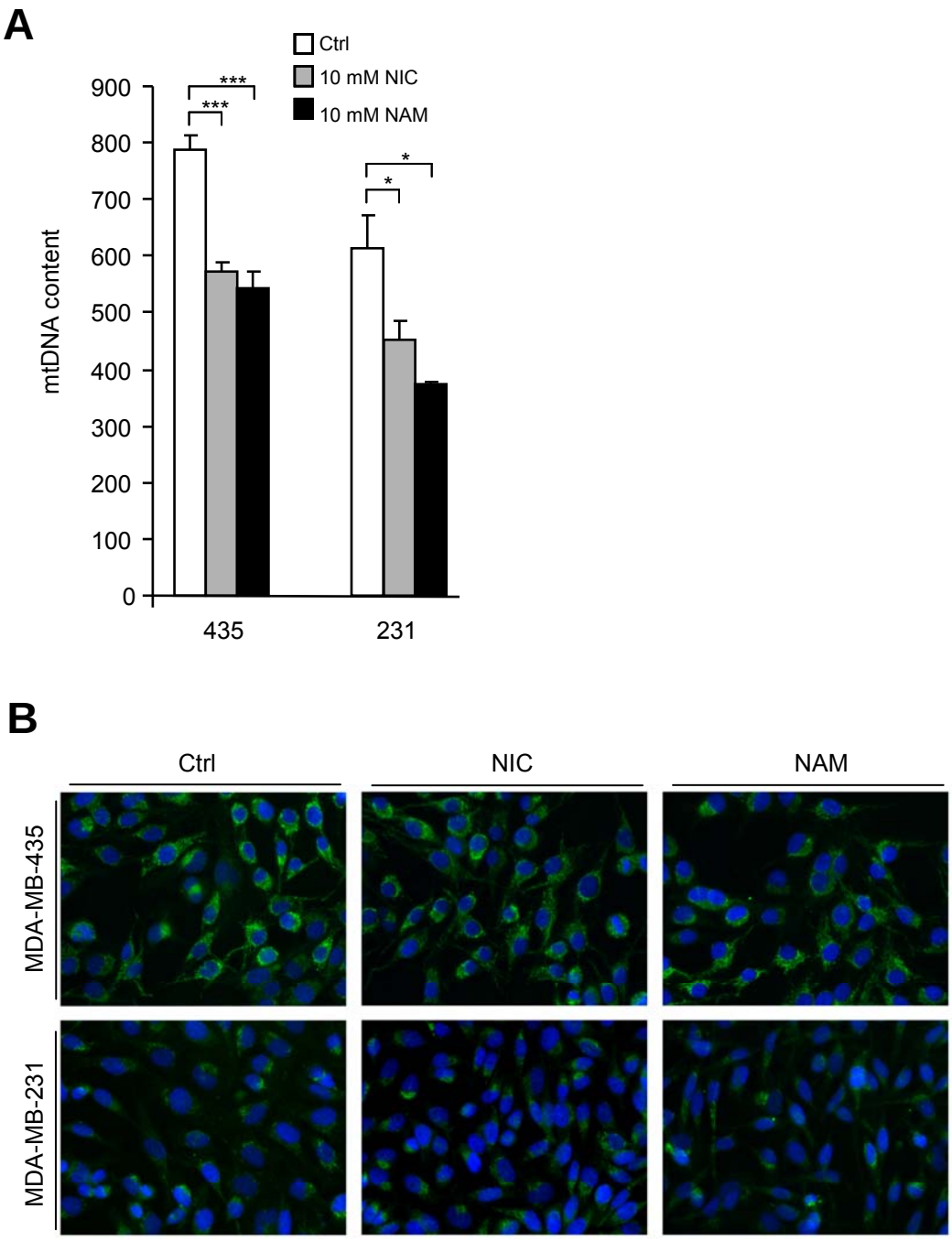

Figure S15. NAD$^+$ precursor treatment induces mitophagy

(A) NAD$^+$ precursor treatment induces mitophagy in cultured MDA-MB-435 and MDA-MB-231 parental cells. mtDNA content was measured after 3 days of cell treatment with 10 mM nicotinic acid (NIC) or nicotinamide (NAM) in complete medium. mtDNA content was analyzed by quantitative real time PCR and referenced to nuclear genomic DNA. Groups were compared by unpaired two-tailed Student's *t*-test in n=2 independent experiments (*P<0.05). **(B)** NAD$^+$ precursor treatment does not change mitochondria distribution in MDA-MB-435 and MDA-MB-231 cancer cells shown by immunocytochemistry. Mitochondrial complex-III localization was measured after 3 days of cell treatment with 10 mM nicotinic acid (NIC) or nicotinamide (NAM) in complete medium.

A

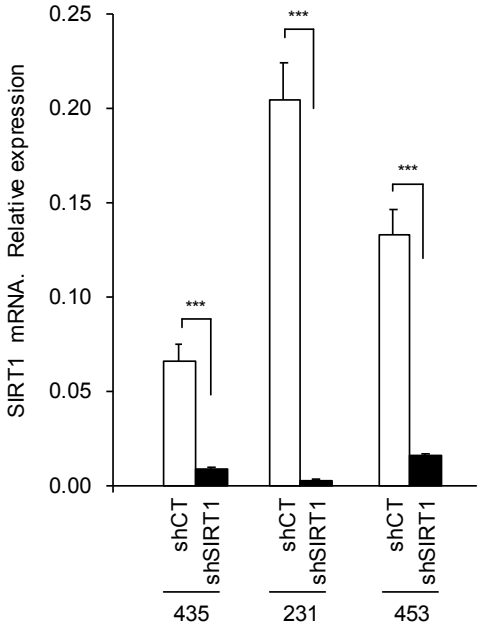

B

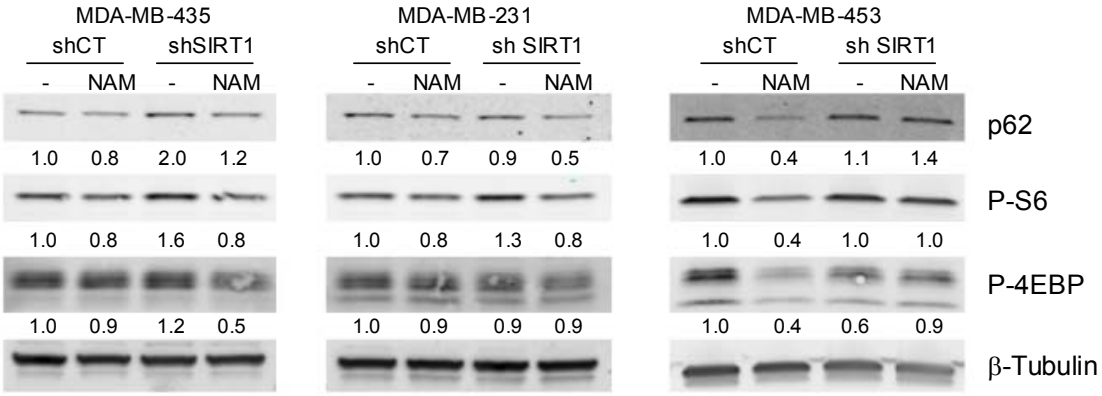

Figure S16. Modulation of mTOR and autophagy by nicotinamide treatment depends on SIRT1 in MDA-MB-453 but not in MDA-MB-435 and MDA-MB-231 breast cancer cells

(A) Lentiviral vectors containing shRNA against SIRT1 (shSIRT1) (clone TRCN0000218734, Sigma-Aldrich, MO) induced stable SIRT1 knockdown and significantly reduced SIRT1 mRNA levels by 86 % in MDA-MB-435, by 99 % in MDA-MB-231 and by 88 % in MDA-MB-453 cells, compared to controls transduced with scrambled shRNA (shCT). SIRT1 mRNA levels were analyzed by real time PCR (probe Hs01009005_m1, Sigma-Aldrich, MO) and expressed relative to β-Glucuronidase (probe Hs99999908_m1, Sigma-Aldrich, MO) (***P<0.001) (n = 3). **(B)** Western blot analysis for p62, and mTORC1 kinase related substrates phospho (Ser240/244)-S6 and phospho (Thr37/46)-4EBP in MDA-MB-435, MDA-MB-231 and MDA-MB-453 SIRT1 knockdown (shSIRT1) vs control (shCT) cells untreated or treated with 10 mM nicotinamide (NAM) for 48 hours. β-tubulin: protein loading control. Signal quantification based on infrared imaging shown at the bottom of each blot.

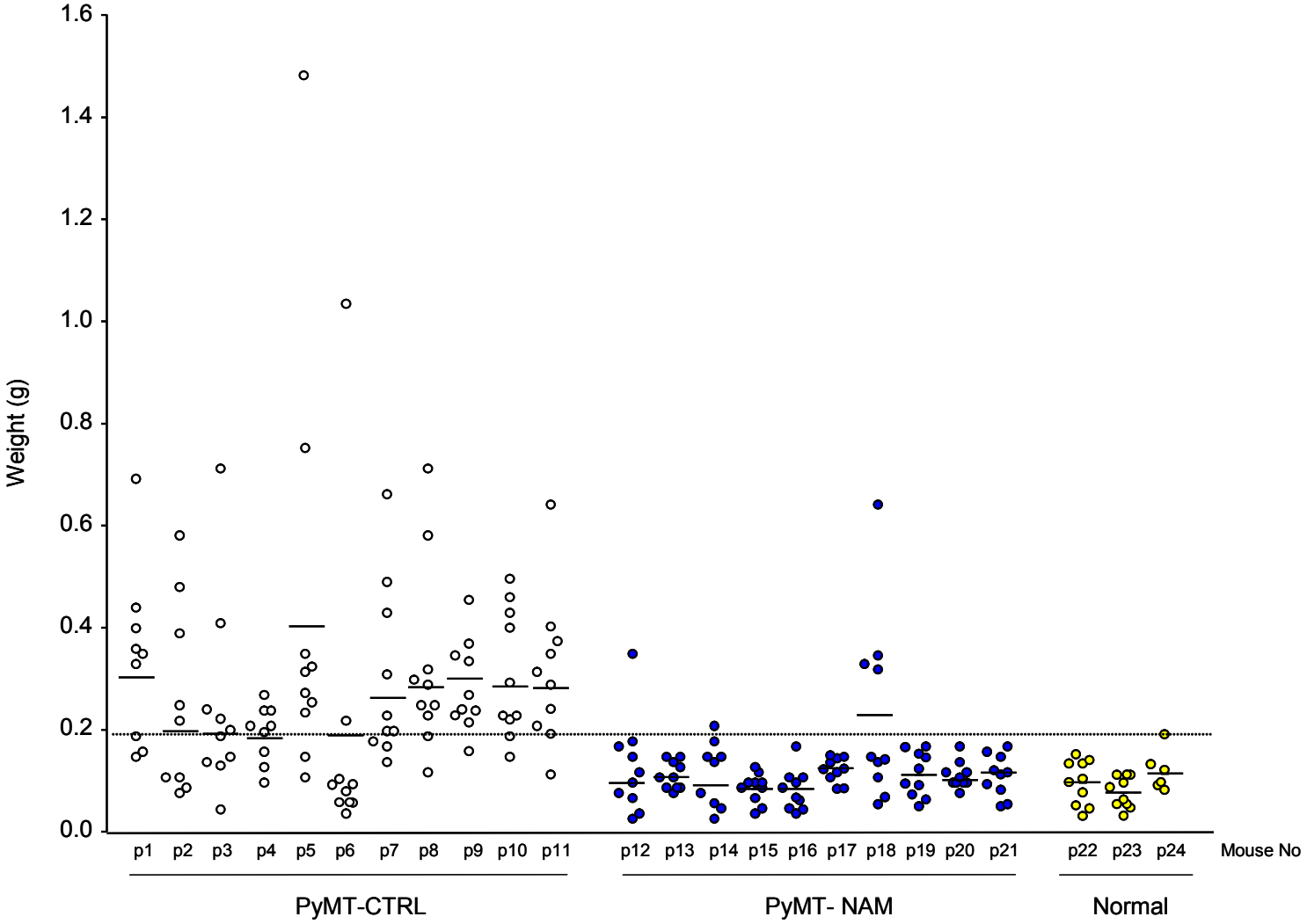

Figure S17. Treatment of MMTV-PyMT mice with NAD$^+$ precursor nicotinamide inhibits spontaneous breast tumor development

MMTV-PyMT mice (strain MT634) were left untreated (PyMT-CTRL) or treated with 1% nicotinamide (PyMT-NAM) in the drinking water at weaning on day 22 and throughout the experiment. Weight of each of 10 mammary fat pads from every mouse on day 80. PyMT-CTRL (n=11), PyMT-NAM (n=10), Normal (untreated non-transgenic mice) (n=3). For every mouse (x-axis), the weight of each individual mammary fat pad (total of 10) is represented. Solid horizontal lines represent the mean fat pad weight for each mouse. Dotted line indicates the maximum weight of a normal mammary fat pad.

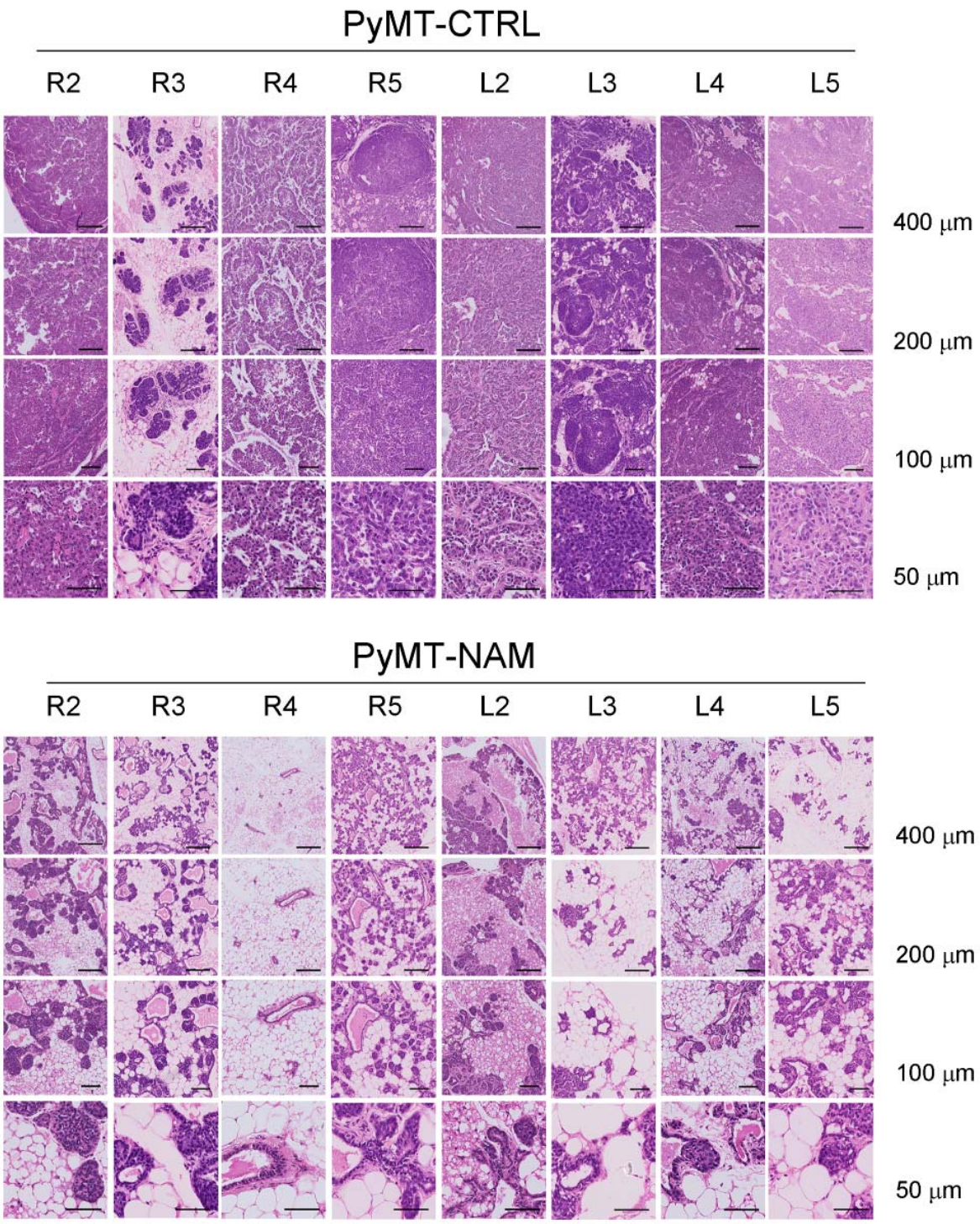

Figure S18. Treatment of MMTV-PyMT mice with NAD^+ precursor nicotinamide inhibits spontaneous breast cancer progression

Representative images of the histology of 8 tumors from untreated (PyMT-CTRL) vs nicotinamide treated mice (PyMT-NAM) on day 80. Treatment with 1% NAM in the drinking water started at weaning on day 22 and continued throughout the experiment. Designation of fat pad location is given at the top of each column: R2 = second right, etc, L2 = second left, etc. Each column shows the same tumor at increasing magnifications (H&E staining). Numbers on the right indicate length of space bars.

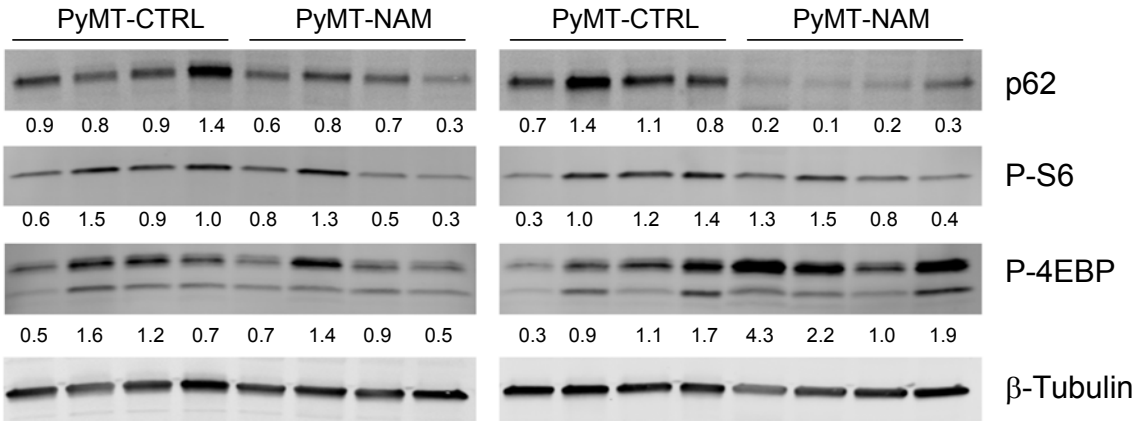

Figure S19. Nicotinamide treatment induces autophagy *in vivo* as seen in the MMTV-PYMT breast cancer mouse model

MMTV-PyMT mice were left untreated (PyMT-CTRL), or treated with 1% NAM (PyMT-NAM) in the drinking water beginning at weaning on day 22 and throughout the experiment. Tumors were harvested on day 80 and analyzed for p62 and mTORC1 kinase related substrates phospho (Ser240/244)-S6 and phospho (Thr37/46)-4EBP by Western blot. N=8 individual mammary fat pads were analyzed from each group. β-tubulin: protein loading control. Signal quantification relative to controls indicated at bottom of blots (measured by infrared imaging).

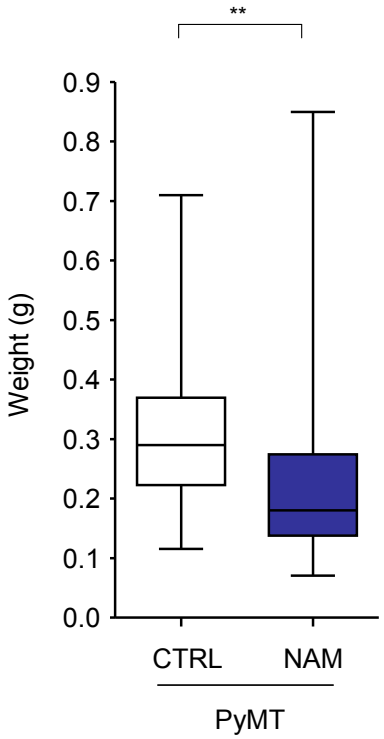

Figure S20. NAD$^+$ precursor treatment of MMTV-PYMT mice with established mammary fat tumors delays breast cancer progression

MMTV-PyMT (PyMT) mice were left untreated (CTRL) (n= 4), or treated with 1% nicotinamide (NAM) (n= 7) in the drinking water beginning on day 60 after palpable tumors had established in each animal. The weight of all 10 mammary fat pads/tumors from every mouse was measured. In box plots, top line denotes the 75% quartile, bottom line the 25% quartile, middle line the median, and whiskers the minima and maxima. Groups were compared by nonparametric Mann-Whitney test (** P<0.01).

Reference List

1. Hofhaus,G., Shakeley,R.M., & Attardi,G. Use of polarography to detect respiration defects in cell cultures. *Methods Enzymol.* **264**, 476-483 (1996).

2. Seo,B.B. *et al.* Molecular remedy of complex I defects: rotenone-insensitive internal NADH-quinone oxidoreductase of Saccharomyces cerevisiae mitochondria restores the NADH oxidase activity of complex I-deficient mammalian cells. *Proc. Natl. Acad. Sci. U. S. A* **95**, 9167-9171 (1998).